Development of direct laser printable light-powered nanocomposites

Ling Chen[a], *Yuqing Dong*[a], *Chak Y. Tang*[a,b,*], *Lei Zhong*[c], *Wing-Cheung Law,*[a,b], *Gary C. P. Tsui*[a,b], *Yingkui Yang*[d], *and Xiaolin Xie*[e]

[a] Department of Industrial and Systems Engineering, The Hong Kong Polytechnic University, Hong Kong, China

[b] Advanced Manufacturing Technology Research Centre, The Hong Kong Polytechnic University, Hong Kong, China

[c] School of Chemistry and Chemical Engineering, Guangxi Key Laboratory Cultivation Base for Polysaccharide Materials and Modifications, Guangxi University for Nationalities, Nanning, China

[d] School of Chemistry and Materials Science, South-Central University for Nationalities, Wuhan, China

[e] School of Chemistry and Chemical Engineering, Huazhong University of Science and Technology, Wuhan, China

ABSTRACT

Four-dimensional (4D) printable light-powered materials have emerged as a new generation of materials for the development of functional devices. The design of these types of materials is mostly based on the *trans-cis* transformation of azobenzene moieties in a liquid crystalline elastomer (LCE) matrix, in which the motion is triggered by ultraviolet (UV) irradiation. In this paper, we first report on a direct laser printable photoresist for producing light-powered 4D structures with enhanced mechanical properties and near-infrared (NIR) responsive mechanical deformation. The reported nanocomposite design is based on the photothermal effects of gold nanorods (AuNRs), which can induce the nematic-to-isotropic (N-to-I) transition of LCE upon exposure to NIR irradiation. The miscibility between AuNRs and LCE is enhanced by thiol-functionalization. Appropriate printing parameters are determined, and nanocomposites containing 0–3 wt.% of AuNR loading are fabricated via femtosecond two-photon direct laser writing (DLW). The effects of the AuNR loading fraction and laser power on the light-powered actuating performance are evaluated. It is found that the nanocomposite with AuNR loading of 3 wt.% demonstrates the maximum percentage (20 %) of elongation under an NIR laser power of 2 W. An increase in laser power can lead to faster deformation but slower restoration. The nanocomposites demonstrate relatively good stability. Even after 300 actuation cycles, 80 % of the elongation magnitude can be retained. In addition, an improvement of 80 % in the complex modulus of the nanocomposites, due to the inclusion of AuNRs, is observed.

1 INTRODUCTION

In recent years, considerable attention has been focused on the advanced three-dimensional (3D) micro/nanofabrication of functional devices with specified functions, including patterned

surfaces for the control of axonal outgrowth and the investigation of the axon mechanobiology,[1] structural metamaterials with ductile-like deformation and recoverability,[2] and induced pluripotent stem cell-derived scaffolds for the treatment of retinal degenerative diseases.[3] Two-photon polymerization (TPP) lithography is one of the direct laser writing (DLW) techniques. By making use of a near infrared (NIR) femtosecond laser and UV curable photoresists, the TPP technique acts as a powerful tool for manufacturing more delicate 3D functional micro/nanodevices with high throughput and high resolution.[4] The photoresists, consisting of monomers or oligomers and photoinitiators, are critical materials for prototyping micro/nanostructures with functionalities. To this end, the photoinitiator should be able to absorb two photons efficiently and generate free radicals or cations, which can initiate the polymerization of the monomers or oligomers and realize the designs. Since the introduction of acrylate photopolymer as the first photoresist suitable for TPP,[5] many other materials, such as SU-8,[6] hydrogels,[7] and organic-inorganic hybrid ORMOCER®[8] have been developed and realistically applied for the fabrication of microscaffolds for cell cultures, the generation of spiral photonic crystals and the building of microcapacitors.[9] Currently, there is growing interest in developing new photoresist materials with free-form printability and various tailored properties for TPP. These materials are direct laser printable 3D structures and can be responsive to external stimuli such as chemical signals, light, heat or pH value (i.e., 4D feature). For example, cleavable photoresists, which can be triggered by a mild chemical signal, have been synthesized to achieve facile removal of microprinted structures.[10] There have also been a few reports on the design of 4D printable photoresists for the construction of light-induced microrobotic structures and light-tunable photonic devices.[11,12] However, most of these designs are based on liquid crystalline elastomers (LCEs) incorporated with azobenzene units.

Light-activated LCEs have attracted increasing attention because they use clean energy and can activate devices at a remote distance in both dry and wet environments.[13] LCEs are cross-linked polymers combining the entropy elasticity of polymeric elastomers and the self-organization of liquid crystalline mesogenic moieties.[14] When LCEs respond to external stimuli, the orientation order of the mesogens is changed, resulting in a macroscopic shape change, and this aspect makes LCEs attractive materials in the development of a new generation of actuating, sensing and robotic devices.[15–18] The incorporation of azobenzene units, which are able to undergo the *trans-cis* isomerization process when exposed to ultraviolet (UV) radiation, into the LCE networks is the most common approach for producing light-responsive LCEs.[18] Azobenzene-containing LCE devices can help realize various types of motions such as contraction,[15] rolling,[19] bending,[20,21] swimming[22] and walking.[11] Most of these devices were fabricated using the soft lithography method, and such devices were often limited to 2D and 2.5D structures (e.g., pillar, cylinder, fiber and thin film), until Zeng et al.[23] successfully used DLW to fabricate UV-driven LCE microstructures. However, the light actuation performance and the mechanical properties of the 3D microstructures have not been discussed extensively.

One major concern regarding azobenzene-containing LCEs is the use of a UV light source. The high energy level of UV light can damage soft tissues, and excessive exposure to UV light has profound risks for human health. Compared to UV light, NIR light has a lower energy level; moreover, NIR light can penetrate deeper and causes less photodamage to tissues and cells.[24] Therefore, it could act as a more suitable stimulus for actuators and microrobotic devices. NIR responsive LCEs have become an important research topic in the LCE community. The incorporation of upconversion materials into azobenzene-containing LCEs is one of the strategies to develop NIR responsive LCEs.[25,26] However, due to the low conversion rate of the

upconversion materials, a high-power excitation of the laser is required, which may cause overheating and limit the applications of the LCEs. Recently, another system, which uses photothermal effects to transform photons into thermal energy and induces nematic-to-isotropic (N-to-I) phase transition of LCEs, has been developed. In this system, nanomaterials with photothermal properties, such as carbon nanotubes (CNTs),[27] graphene oxide (GO),[28] and graphene,[29] play essential roles for providing photoactuation in LCEs. The CNT/LCE nanocomposite films fabricated by Yang et al.[30] demonstrated a reversible contraction strain of 30 % in four seconds under IR radiation. GO, which has a high thermal conductivity and photothermal conversion capability,[31] was incorporated into an LCE, resulting in a photothermal actuating nanocomposite film with a contraction ratio of 33 %[32]; however, the contraction appeared to be irreversible, and an external weight was required to be provided to recover the shape. Moreover, it has been reported that the moduli of TPP fabricated materials are often smaller than that of bulk materials prepared via UV irradiation.[33–35] The incorporation of nanomaterials can not only toughen the LCE but can also improve their thermomechanical and photothermal properties.

Gold nanoparticles (AuNPs) such as gold nanospheres (AuNSs) and gold nanorods (AuNRs), with tunable localized surface plasmon resonance (LSPR) properties, can efficiently and rapidly convert photon energy to thermal energy. It has been reported that the optical absorption cross-section of AuNPs is much higher than that of CNTs, which can facilitate photothermal conversion and induce rapid mechanical response upon laser irradiation due to the incorporation of only a small amount of AuNP into LCEs.[36] Moreover, gold with high thermal conductivity can increase the thermal conductivity of LCEs and enhance their thermomechanical properties.[37] AuNP-doped LCE microcylinders have been robustly controlled via a scanned laser beam.[38]

AuNR/LCE composite micropillars with a reversible photothermal actuation demonstrated a 30 % higher maximum light-induced strain than that of the AuNS/LCE ones.[36] An irreversible NIR responsive AuNR/LCE composite fiber was fabricated using sequential thiol-click chemistry that stabilized the AuNRs and improved the miscibility between the AuNRs and LCEs.[39] To the best of our knowledge, these AuNR/LCE nanocomposite are usually fabricated based on UV photopolymerization and in the forms of pillar, cylinder, fiber and thin film instead of complex 3D structures. TPP has rarely been used for the fabrication of AuNR/LCE nanocomposites, and there has been no systematic study on their printability, light-induced performances and mechanical properties. The challenges of combining TPP with AuNR/LCEs include the following:

(1) Design of a TPP laser printable photoresist with suitable liquid crystal monomer, crosslinker and photoinitiator;

(2) Improvement in the miscibility between the AuNRs and developed photoresist;

(3) Ensuring the occurrence of a nematic liquid crystal phase (long-range orientation of liquid crystal mesogens) during the TPP DLW process; and

(4) Determination of the appropriate printing parameters, as AuNRs with high photothermal effect can easily cause overheating and damage the entire structure.

This paper reports on a laser direct printable AuNR-modified nanocomposite with reversible and rapid NIR actuation. In contrast to previously reported LCE composites fabricated using conventional soft lithography with 2D/2.5D structures, TPP DLW was used, for the first time, to synthesize and fabricate AuNR-modified LCEs with 3D microstructures. To perform the TPP DLW, LCMs and a crosslinker with acrylate moieties, which demonstrated transparency at 780 nm (TPP laser wavelength) and 390 nm (two-photon absorption wavelength), were selected. A

photoinitiator with an absorption window of approximately 300–400 nm, transparent at wavelengths of more than 700 nm, was selected to absorb photons and trigger a chain reaction. Surface functionalization of AuNRs was used to improve the dispersion of AuNRs in LCM. AuNR/LCE nanocomposites with different 3D structures were fabricated using TPP DLW. In addition, the actuation properties of a nanocomposite with a 3D photonic woodpile microstructure were investigated. Jumping out of the "azo-requirement box" and using the photothermal effect of AuNRs, the micro-actuator developed to have remote triggering capability can perform rapid and reversible shape deformation via NIR laser irradiation. This aspect broadens the device's potential applications in biomedical engineering, optomechanics, microfluidics, and micro/nanoelectromechanical (MEMS/NEMS) systems. The effects of both the laser power and AuNR loading ratio on the photothermal actuation of the AuNR/LCE nanocomposite were investigated. A multicycle actuation test was performed to study the long-term stability of the AuNR/LCE nanocomposites. Nanodynamic mechanical analysis was carried out to study the effect of AuNR loading amounts on the mechanical properties of the nanocomposites. We believe that the study can provide novel approaches for designing and fabricating high-performance light-powered 4D printable nanocomposite micro- and nano-actuating devices.

2 EXPERIMENTAL SECTION

2.1 Materials

Hydrogen tetrachloroaurate trihydrate ($HAuCl_4 \cdot 3H_2O$), hexadecyltrimethylammonium bromide (CTAB, 98 %), and 3-mercaptopropionic acid were purchased from Macklin, China. Hydroquinone (99 %) was purchased from Tokyo Chemical Industry Co., Ltd, Japan. Silver nitrate ($AgNO_3$, 99 %), sodium borohydride ($NaBH_4$, ≥96 %), propylene glycol monomethyl

ether acetate (PEMGA, 99 %) and the photoinitiator Irgacure 369 were purchased from Sigma-Aldrich, USA. The liquid crystal monomers (LCMs), 1, 4-Bis-[4-(3-acryloyloxypropyloxy) benzoyloxy]-2-methylbenzene (RM257) and 4-Methoxybenzoic acid 4-(6-acryloyloxy-hexyloxy) phenyl ester (C6BP) were purchased from SYNTHON Chemicals GmbH & Co. KG, Germany. The polyimide (PI)-based aligner (DL-2590) was purchased from Shenzhen Dalton Electronic Material Co., Ltd., China.

2.2 Synthesis and Characterization of AuNRs and Thiol-Functionalization

AuNRs were prepared using a seed-mediated growth method with small modifications.[40] $HAuCl_4$ solution (5 ml, 0.5 mM) was mixed with 5 ml of CTAB (0.2 M) solution and stirred until the mixture became clear. NaBH4 (0.01 M) was then added dropwise to the mixture under vigorous stirring until the color changed to light brown, and the mixture was left standing for 110 min to obtain a gold seeding solution. $HAuCl_4$ solution (10 ml, 10 mM) was mixed with 200 ml of CTAB (0.1 M) and 1.5 ml of silver nitrate (0.1 M) under stirring for 30 min. Subsequently, 10 ml of 0.1 M hydroquinone aqueous solution was added to the previously mixed solution. The growth process of the AuNRs was initiated after the addition of 2.6 ml of gold seed solution. After overnight aging, the AuNR aqueous dispersion was prepared. A UV/Vis spectrophotometer (UV1102, Techcomp Ltd., China) was used to measure the LSPR peak of the as-synthesized AuNRs. The morphology of the AuNRs was observed via transmission electron microscopy (TEM) (Jeol JEM-2011, Japan).

Immiscibility with LCMs and easy aggregation are the main limitations of AuNRs when used as photothermal fillers.[38,39] To address these shortcomings, AuNRs was treated with 1 % (v/v) 3-mercaptopropionic acid (MPA) ethanol solution by adding 0.5 ml of MPA solution to fresh AuNR aqueous solution with vigorous stirring at 35 °C, followed by stirring for another four

hours. This mixed system was then centrifuged three times at 9000 rpm for 20 min to remove the excess CTAB and MPA and placed into a dialysis bag in a beaker of ethanol for purification. The MPA-capped AuNRs were obtained and redispersed in ethanol with a concentration of 15 mg/ml via ultrasonication.

2.3 Preparation of AuNR/LCM Mixture and Liquid Crystal Cell

LCM mixtures were prepared using C6BP, RM257, and 2 mol% of Irgacure 369, as depicted in Figure 1. The molecular ratio of RM257/C6BP was 1:9. LCM mixtures were dissolved in acetone, and appropriate amounts of MPA-capped AuNRs (1 wt.%, 2 wt.% and 3 wt.%) were dispersed in the LCM acetone solution under sonication. After solvent evaporation, the MPA-capped AuNR/LCMs mixtures were prepared for subsequent DLW of the 3D microstructures. For comparison, 3 wt.% untreated AuNRs were also added into LCMs to characterize the dispersion of AuNRs. Figure S1 shows the change in the color of the LCM mixture after the addition of AuNRs. It is apparent that untreated AuNRs agglomerated critically in the mixture, while no phase separation was observed for the MPA-capped AuNR/LCM mixture. This suggests that the ligand exchange process with MPA facilitates the dispersion of AuNRs in LCMs.

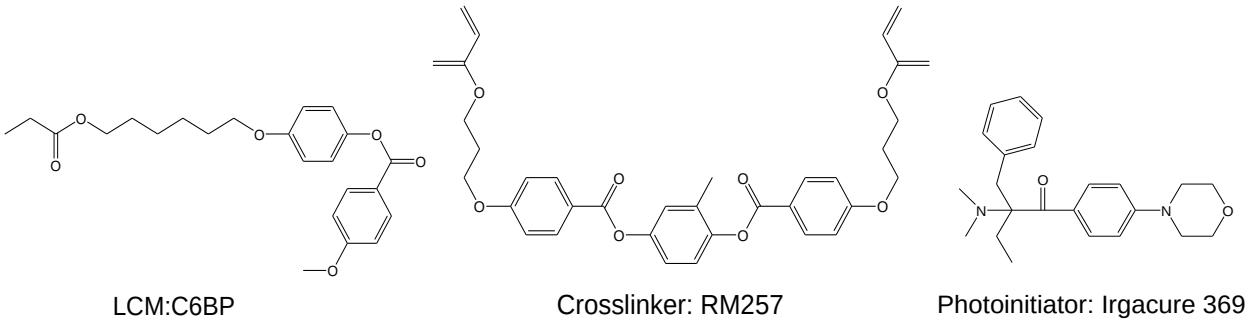

Figure 1. Molecular structures of LCM, crosslinker and photoinitiator.

Before DLW was performed, a liquid crystal cell was prepared to ensure the long-range orientation of the liquid crystal mesogens, which was crucial for the AuNR/LCE to achieve N-to-I phase transition and photomechanical response. In this work, a uniaxial in-plane molecular alignment was prepared to achieve contraction and elongation motions. A planar alignment PI solution was spin coated onto a coverslip at a coating speed of 930 rpm for one minute (Scheme 1a). The coated coverslips were placed on a hot plate at 100 °C for 15 min and baked in an oven at 200 °C for two hours. The alignment layers on the glasses were uniaxially rubbed with a velvet cloth (Scheme 1b). Finally, the liquid crystal cell was developed using two PI coated glasses rubbed in opposite directions with a glass sphere spacer (diameter: 100 μm) placed in-between (Scheme 1c). The AuNR/LCM mixture was placed on the edge of the cell and infiltrated into the cell on a hot plate at 65 °C. As a result, the liquid crystal mesogens were parallel to the cell and pointing to the in-plane direction. A AuNR/LCE film was prepared by exposing the AuNR/LCMs infiltrated liquid crystal cell to a UV light, and it was subsequently examined using a UV/Vis spectrophotometer (UV1102, Techcomp Ltd., China) to study the dispersion state of AuNRs in the LCE matrix.

Scheme 1. Schematic of (a) spinning coating of alignment layer onto a coverslip (b) rubbing the alignment layer in one direction (c) preparation of liquid crystal cell and infiltration of AuNR/LCMs (d) femtosecond DLW of 3D microstructures in the cell via two-photon polymerization

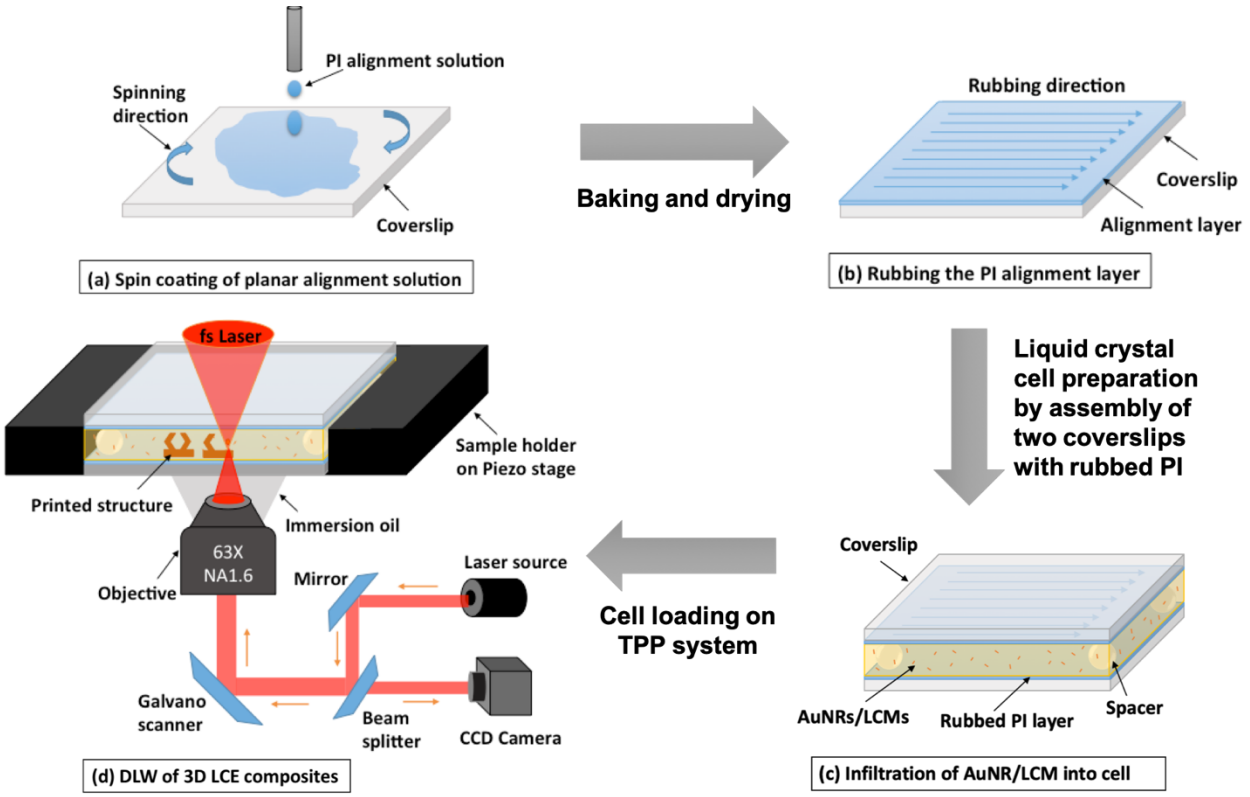

2.4 Direct Laser Writing of AuNR/LCE 3D Microstructures

A commercially available TPP DLW system (Photonic Professional GT, Nanoscribe GmbH, Germany) was used for the fabrication of 3D microstructures. The objective lens had a magnification of 63× with a numerical aperture (NA) of 1.4. The schematic of the DLW process is shown in Scheme 1d. A AuNR/LCM infiltrated cell was transferred to the sample holder and inserted into the TPP lithography system. A drop of immersion oil (NanoScribe GmbH, Germany) was added to the bottom outer surface of the cell. Femtosecond laser pulses with wavelengths of 780 nm were focused on the AuNR/LCM mixture in the cell to induce TPP. To achieve satisfactory orientation of the LC units in the LCE and ensure photomechanical actuation, printing should be performed in a temperature range in which the LCM mixture is in the nematic phase. Differential scanning calorimetry (DSC) (Mettler Toledo, DSC3, Swiss) was used to measure the nematic-isotropic transition temperature (T_{NI}) of the LCMs and AuNR-

modified LCMs. Samples with at least 2 mg of AuNR/LCE were loaded into aluminum pans and heated from room temperature to 100 °C at 20 °C /min. Subsequently, the samples were cooled to -20 °C and later heated to 100 °C at 10 °C/min. Nitrogen was used as the protective gas. The results pertaining to the DSC are shown in Figure S2. The T_{NI} values for unfilled LCM and AuNR/LCM mixtures with 1 wt.%, 2 wt.% and 3 wt.% of AuNRs were 53.9 °C, 53.7 °C, 53 °C and 52.3 °C, respectively. The 3D microstructures were written in accordance with the digital designs within the range of room temperature and T_{NI}. Afterwards, the cell was opened, and the printed structures were developed in acetone for one minute and in isopropanol for another minute to remove any uncured materials.

2.5 Thermogravimetric Analysis of AuNR/LCE Composites

Thermogravimetric analysis (TGA) (Mettler Toledo TGA/DSC3+, USA) was used to determine the actual concentration of AuNRs in the fabricated AuNR/LCE composites. Samples with at least 2 mg of AuNR/LCE were loaded, and tests were carried out under a nitrogen atmosphere at a heating rate of 15 °C/min, from room temperature to 650 °C.

2.6 Morphological Observation

A scanning electron microscope (SEM) (Tescan VEGA3, Czech Republic) was used to observe the fabricated 3D AuNR/LCE structures at an accelerating voltage of 15 kV. The structures were sputter-coated with a gold layer. A polarized optical microscope (POM) (Nikon Eclipse LV 100N POL, Japan) equipped with a CCD camera (Nikon DS-Ri2, Japan) was used to capture the optical images and examine if the LC mesogens in the TPP DLW fabricated AuNR/LCE nanocomposite were well aligned along the rubbing direction, which is essential for light-powered mechanical deformation.

2.7 Nano-Dynamic Mechanical Analysis

A TI 900 triboindenter (Hysitron Inc., USA) equipped with a Berkovich tip was used to perform nanodynamic mechanical analysis (nano-DMA) on the printed AuNR/LCE microplate having the dimensions of 100 μm ×100 μm ×20 μm. Force control and frequency sweep nano-DMA tests were carried out for continuous measurement of the storage modulus (E′), loss modulus (E′′), complex modulus (E^*) and loss factor (tan δ) of the AuNR/LCE at different indent displacements and frequencies, respectively. For the force control tests, the applied force was increased to 150 μN within 30 s, and the probe oscillated at a constant frequency of 220 Hz. In the frequency sweep tests, the peak force was 100 μN with dynamic oscillations of 9 μN. The sweeping frequencies varied from 10 Hz to 300 Hz. Five indents were performed on each sample with a distance of 20 μm between the neighboring indents.

E′ represents the stiffness of a material and its capacity to store energy, while E′′ represents the capacity of a material to dissipate energy. E^* is defined as the ratio of the stress amplitude to the strain amplitude, and it represents the stiffness of a material. Tan δ is defined as the ratio of the loss modulus to the storage modulus, indicating the damping of a viscoelastic material. The following equations can be used to calculate these values:

$$\mathrm{E}' = {K_S\sqrt{\pi}}\Big/{2\sqrt{A}} \tag{1}$$

$$E'' = {\omega C_D\sqrt{\pi}}\Big/{2\sqrt{A}} \tag{2}$$

$$E^* = \mathrm{E}' + iE'' \tag{3}$$

$$tan\delta = {\mathrm{E}''}\Big/{\mathrm{E}'} = {\omega C_D}\Big/{K_s} \tag{4}$$

where A is the contact area between the indenter and the material, ω is the angular frequency, and K_S and C_D denote the elastic stiffness and damping of the contact, respectively, which can be calculated as follows:

$$K_s = \frac{F_0}{Z_0}\cos\phi + m\omega^2 - K_i \quad (5)$$

$$\omega C_D = \frac{F_0}{Z_0}\sin\phi - \omega C_i \quad (6)$$

where F_0 and Z_0 are the force and displacement amplitudes of an oscillating system, respectively; ϕ is the phase shift; and m, K_i and C_i are the mass, stiffness and damping of the indenter, respectively.

2.8 Photothermal Actuation of AuNR/LCE 3D Microstructures

To evaluate the photothermal actuation properties of the TPP DLW fabricated AuNR/LCE 3D microstructures, diode laser irradiation (LSR80H, Lasever Inc., China) with a wavelength of 808 nm and adjustable output laser power from 0.5 W to 2.5 W (power density from 1.5 W cm^{-2} to 7.8 W cm^{-2}) was applied to the specimens. The distance between the laser source and the sample was 25 cm. The actuation processes were observed using a microscope and recorded using a CCD camera. Woodpile structures having an overall size of 140 µm (width) × 140 µm (length) × 20 µm (height) were designed and fabricated via DLW (Figure S3), and they were used as reference structures to study the photothermal actuation properties of AuNR/LCE nanocomposite materials and the shrinkage rate of the structure after development. One edge of the woodpile structure was fixed (marked in red as "fixed end") and attached to the substrate to prevent the structure from being washed away during the development process and to preserve the original dimensions, while the remaining part was loosened from the substrate and was free to move. After development, since the change in the length (y- direction) of the fixed end was negligibly small, this length was considered as the original length and width of the woodpile structure. The length (y- direction) of the free end was reduced by approximately 15 %, and this was considered as the shrinkage rate in the y-direction. The shrinkage rate in the x- direction was calculated to be 15 %. To study the photothermal actuation properties, the dimensional changes in the x- and y-

directions of the structure were measured. The experiments were carried out at room temperature. The photothermal actuation induced shape deformation and the response time of the unmodified LCE and AuNR/LCEs with 1 wt.%, 2 wt.% and 3 wt.% AuNRs were investigated. The effects of both the AuNR loading fraction and laser power on the photothermal actuation were studied. Videos and images were acquired during the actuation process, and the data were analyzed using the *ImageJ* software. The response of three hundred actuation cycles to on–off switching of NIR light at intervals of five seconds was determined to study the long-term actuation stability. In addition, the actuation behaviors of a AuNR/LCE 3D microstructure in the form of a microclamp were recorded.

3 RESULTS AND DISCUSSION

3.1 Morphological Observation and UV/Vis Measurement of AuNRs and AuNR/LCE Film

The TEM images of the as-synthesized AuNRs are shown in Figure 2a. The aspect ratio of AuNRs with a width of 10 nm was estimated to be 4.6. The monodispersed AuNRs were stable in water, and no precipitation was observed even after several weeks. The UV/Vis spectra of the as-synthesized AuNRs and UV-cured AuNR/LCE film are shown in Figure 2b. Both spectra demonstrated two LSPR bands located at 514 nm and 810 nm, which could effectively convert the photon energy at 810 nm to heat energy. Band broadening and redshifting were observed in the AuNR/LCE film, likely due to a change in the dielectric environment of the AuNRs in LCE.[36,41] Figure S1 shows that no obvious aggregation occurred in the AuNR/LCM mixture solution.

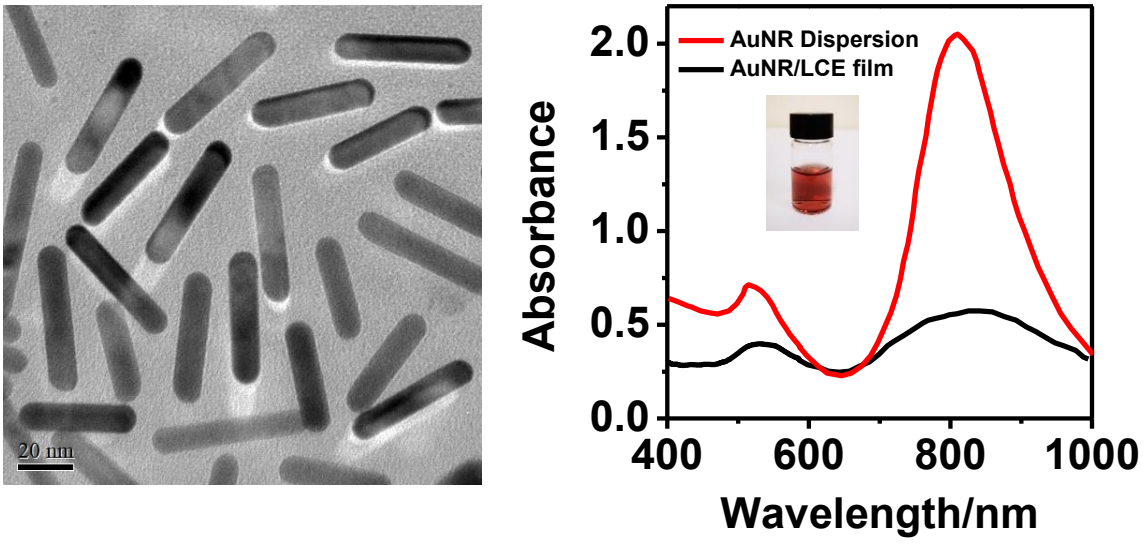

(a) (b)

Figure 2. (a) TEM images of AuNRs and (b) UV-Vis spectrum of as-synthesized AuNR aqueous dispersion and UV cured AuNR/LCE film (Inset: Photograph of AuNR aqueous dispersion).

3.2 Determination of Printing Parameter for AuNR/LCM 3D Microstructures

The working range of TPP must be carefully determined because the laser power must be (1) larger than the polymerization threshold to initiate polymerization and (2) smaller than the burning threshold to prevent the breakdown of the material.[42] Our aim was to set the printing parameters such that a high polymerization rate of the LCE could be ensured without shape distortion and burning of the structure. The LSPR characteristic of AuNRs leads to the efficient absorption of NIR photons and conversion into a large amount of thermal energy in a very short period of time during the TPP printing process, which causes bubbling of the photoresist and localized burning of the printed structure. Using a low laser power can reduce this effect, but it may lead to incomplete polymerization of the LCEs. This makes the printing process more difficult than when employing DLW of LCMs with azobenzene units.[23] Moreover, it has been

reported that the mechanical properties, such as the Young's modulus, of the materials fabricated using TPP DLW are usually smaller than those of the bulk materials prepared using UV irradiation.[33–35] Therefore, it is important to determine an optimum condition for obtaining a satisfactory quality of AuNR/LCE 3D microstructures with mechanical properties closer to that of the bulk ones. In this case, a pyramidal structure was designed as the model printing structure (Figure 3). The laser power was adjusted to be in the range of 2.5–42.5 mW, and the scanning speed was varied from 1 mm/s to 9 mm/s. It was found that the loading amount of AuNRs could affect the writing process. The effective working range (reasonable combinations of scanning speeds and laser powers) was reduced with increase in the amount of AuNRs. Parameter sweeping was conducted for AuNR/LCM with AuNR loading amounts of 1–3 wt.%. When the AuNR filling amount increased to 4 wt.%, no suitable printing parameters could be found. Therefore, Figure 3 shows the parameter sweeping results of 3 wt.% AuNR/LCM, which can also be applied to fabricate nanocomposites with 1–2 wt.% AuNR filling amounts. Eighty-one pyramidal structures with different parameters were printed. Eight structures were considered as failures due to unsuccessful polymerization. An effective printing area with appropriate ranges of laser powers and scanning speeds and noted to have an acceptable resolution was determined. The resolution is defined as the degree of detail that can be seen with acceptable clarity, i.e., four clear lateral truss members. If these details cannot be seen, the printed structures are considered as having unacceptable resolution. The lateral spatial resolution of TPP was reduced by increasing the laser power or reducing the scanning speed, as suggested by Xing's group.[43] Figure 3 shows that the laser power should be in a range of 7.5–17.5 mW for printing pyramidal structures with acceptable resolution. At a high laser power (17.5 mW) the details of the structure were compromised. When the power was greater than 32.5 mW (above the burning

threshold), the generated heat flux caused bubbling and localized explosion or burning, resulting in the destruction of the samples. Based on the results from the parameter sweeping process, a power of 12.5 mW and a scanning speed of 9 mm/s were chosen for further fabrication of the samples.

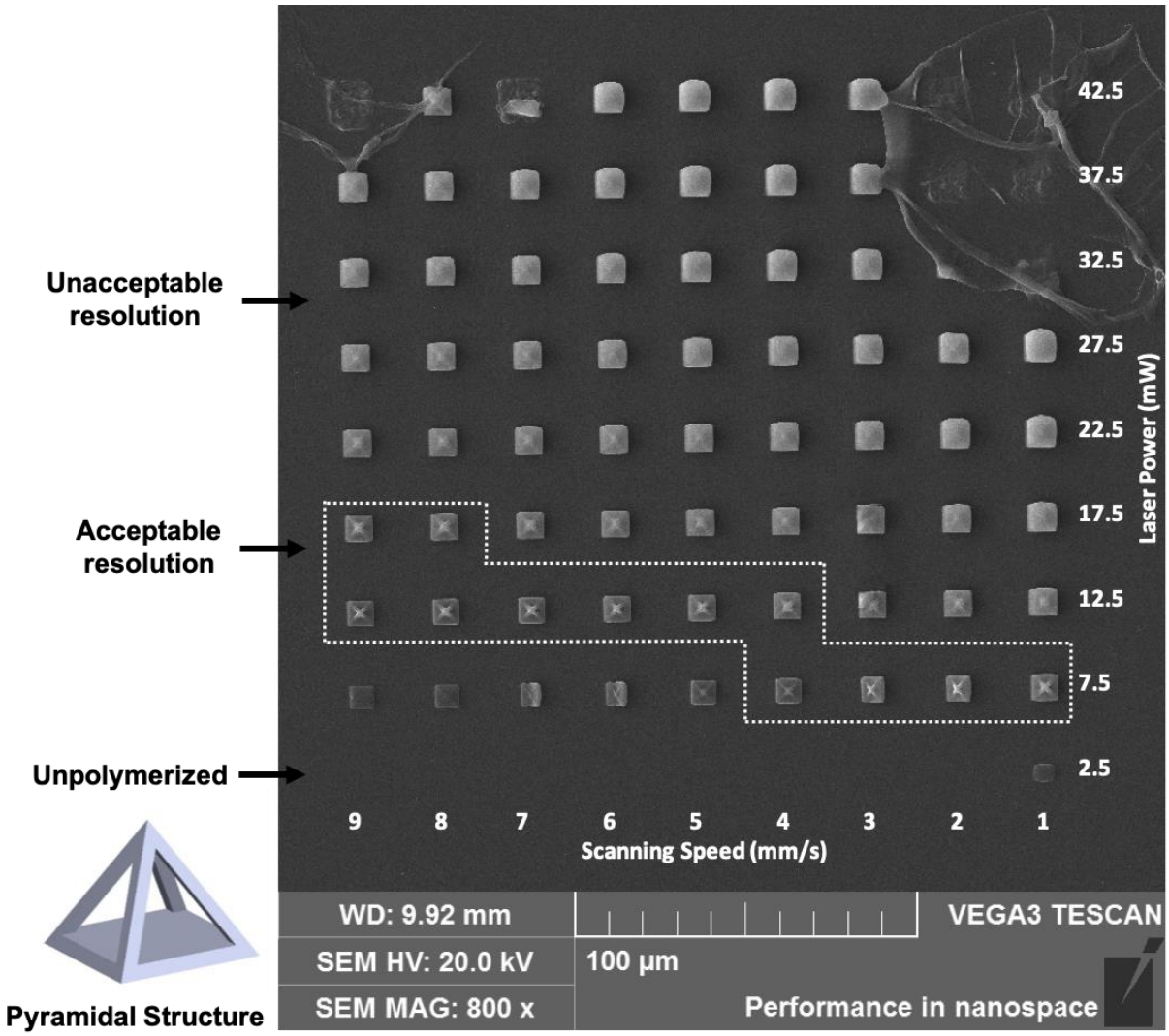

Figure 3. Three-dimensional model of pyramidal structure and SEM images of AuNR/LCE nanocomposite structures fabricated using TPP. The AuNR loading fraction is 3 wt.%. The structures are fabricated using laser powers ranging from 2.5 to 42.5 mW (bottom to top) and scanning speeds ranging from 1 to 9 mm/s (right to left).

3.3 Thermogravimetric Analysis of AuNR/LCE Composites

TGA was used to confirm the actual concentration of AuNRs in the fabricated AuNR/LCE composites. The results for the variation of residual mass with temperature for AuNR/LCE composites are shown in Figure S4. It was found that the thermal degradation of LCE commenced at approximately 200 °C and terminated at approximately 500 °C. The TGA results indicated that the actual loadings of AuNR were estimated to be 1.4 wt.%, 2.2 wt.% and 3.5 wt.%, corresponding to the initial loadings of 1 wt.%, 2 wt.%, and 3 wt.%, respectively. This finding suggested that the preparation method did not lead to any loss of AuNRs during the preparation.

3.4 Confirmation of the Alignment of Liquid Crystal Mesogens via POM

POM was used to confirm the alignment of LC mesogens in the printed AuNR/LCE along the rubbing direction. The POM images (Figure 4) revealed a high level of molecular alignment along the rubbing direction of the PI layer in the printed structure. When the rubbing direction of AuNR/LCE sample was parallel or perpendicular to the analyzer, the transmittance was minimized. As a result, the sample could hardly be seen, as in Figure 4a. The image given as Figure 4b was captured when the sample was rotated at an angle of 45° to the analyzer, in which case, the transmittance of the sample was maximized. The homogenous planar alignment of the LC mesogens in the printed microstructures contributes considerably to the photothermal actuation performance, as the aligned mesogens (nematic phase) can transform into an unordered state (isotropic phase) upon NIR irradiation, inducing a change in the shape of the microstructures.

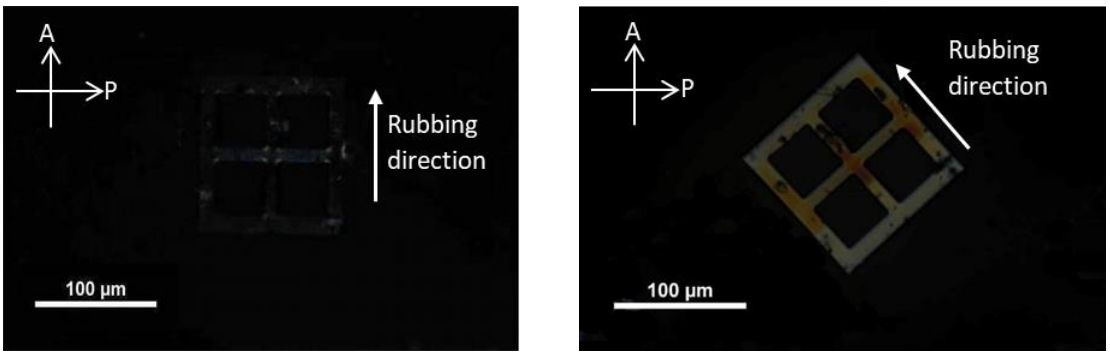

(a) (b)

Figure 4. Polarized optical microscope images of a fabricated structure (a) structure parallel to the analyzer (b) structure at an angel of 45° to the analyzer.

3.5 Nanodynamic Mechanical Analysis

Both force control and frequency sweep nano-DMA tests were used to determine the mechanical properties of the printed AuNR/LCE nanocomposites. The values of E', E'', E^*, and tan δ at an indent displacement of 250 nm, obtained from the force control tests, are summarized in Table 1. All samples had larger E' values than E'' values, demonstrating better elastic behavior than viscous behavior. The LCEs modified with AuNRs demonstrated higher E', E'' and E^* values than the unmodified one. These values increased with increase in the amount of AuNRs. The results indicated that AuNRs significantly improved the mechanical properties of the LCEs by more than 80 % compared to the performance of the unfilled LCEs. No significant difference existed in the values of the loss factor for the samples. The values of E', E'', tan δ and hardness (H) of the AuNR/LCE and unmodified LCE as a function of frequency are shown in Figure 5. It is clear that E' and H increased while E'' decreased with increase in the indent frequency from 10 Hz to 300 Hz (Figures 5a, b and d). The AuNR/LCE demonstrated higher values of E', E'' and H compared to those of the unmodified LCE within this frequency range, but no significant

different in tan δ existed among the four LCE samples (Figure 5c). It was noted that the increase in E′, E″ and H depended on the increase in the AuNR concentration. These results were consistent with those from the force control tests. When the indent frequency was 300 Hz, the storage moduli of 3 wt.%, 2 wt.%, and 1 wt.% AuNR/LCE were 129 %, 171 % and 200 % those of the unmodified LCE, respectively. The hardness of 3 wt.% AuNR/LCE was noted to increase to 3.7 times that of the unmodified one. This increase indicated that the AuNRs, acted as an inorganic nanofiller, strengthened the LCE and significantly enhanced its mechanical properties.

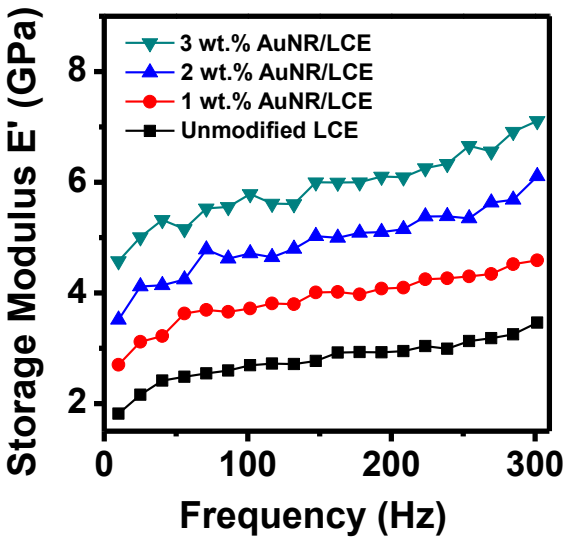

(a)

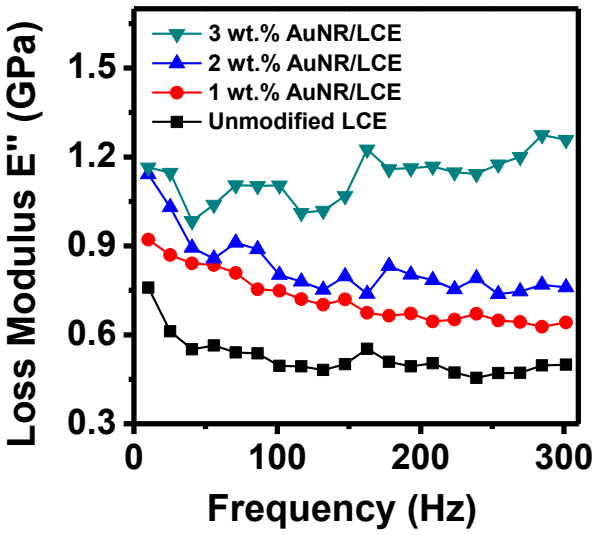

(b)

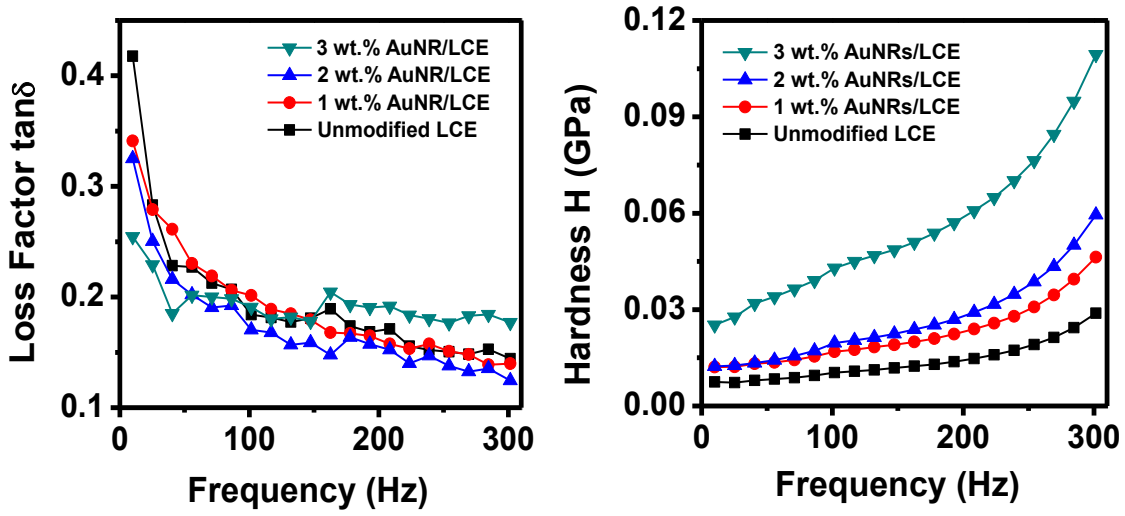

(c) (d)

Figure 5. (a) Storage modulus, (b) loss modulus, (c) loss factor and (d) hardness of AuNR/LCE and unmodified LCE as a function of frequency from nano-DMA.

Table 1. Summary of Mechanical Properties of the Printed LCE and AuNR-Modified LCE at Indent Displacement of 250 nm

Samples	Storage modulus (E', GPa)	Loss modulus (E'', GPa)	Complex modulus (E^*, GPa)	Loss factor (Tan δ)
Unmodified LCE	3.14±0.08	0.43±0.02	3.17±0.08	0.14±0.01
LCE with 1 wt.% AuNRs	3.49±0.59	0.56±0.08	3.53±0.60	0.16±0.01
LCE with 2 wt.% AuNRs	4.42±0.11	0.74±0.03	4.49±0.11	0.17±0.01
LCE with 3 wt.% AuNRs	5.86±0.42	0.91±0.06	5.93±0.43	0.16±0.01

Over the past few decades, many studies focused on nanocomposite materials have reported that the mechanical properties of polymers can be improved by the addition of nanofillers,[44–47] and some reinforcement models, such as the jamming theory[48] and retardation of polymer

dynamics,[49] have been developed to explain the reinforcing mechanisms. The jamming theory states that the reinforcement is the response of a polymer to the drag friction caused by particles. In our case, the increase in the modulus was not caused by jamming due to the low concentration of AuNRs (1–3 wt.%). Furthermore, the retardation of polymer dynamics in the interfacial zone around the nanoparticles can explain the reinforcement effect of AuNRs.[48] The movements of polymer chains slow down since the polymer–particle interaction energy is larger than the polymer–polymer interaction energy, which results in an increase in the modulus that is positively correlated to the volume fraction of the interfacial zone. The volume fraction of the interfacial zone is increased in accordance with the filling ratio of the nanoparticles. This retardation polymer dynamics in the interfacial zone model can be used to explain our nano-DMA results, i.e., increase in the modulus with increase in the AuNR fraction.

3.6 Photothermal Actuation of the AuNR/LCE 3D Microstructures

The mechanism of the reversible shape changing behavior of the AuNR/LCE induced by the photothermal effect of the AuNRs is illustrated in Scheme 2. When the AuNR/LCMs are infiltrated into the liquid crystal cell, the LC mesogens are aligned along the rubbing direction (x-direction) of the PI alignment layer, in a nematic phase (Scheme 2a). In the DLW process, the LCMs are crosslinked via TPP and converted into LCEs, while the LC mesogens still maintain a decent order (Scheme 2b). Due to the NIR laser stimulation, the AuNRs in the LCE network convert the photon energy to thermal energy, which increases the temperature of the AuNR/LCE. When the temperature reaches T_{NI}, LCE becomes isotropic by undergoing a N-to-I phase transition, in which the aligned LC mesogens become disordered. As illustrated in Scheme 2c, contraction occurs along the rubbing direction, while elongation occurs in the transverse

direction. When the NIR laser is removed, the AuNR/LCE nanocomposite can return to its original shape.

Scheme 2. Schematics of the Mechanism of the Reversible NIR Responsive Shape Deformation Behavior of the AuNR/LCE

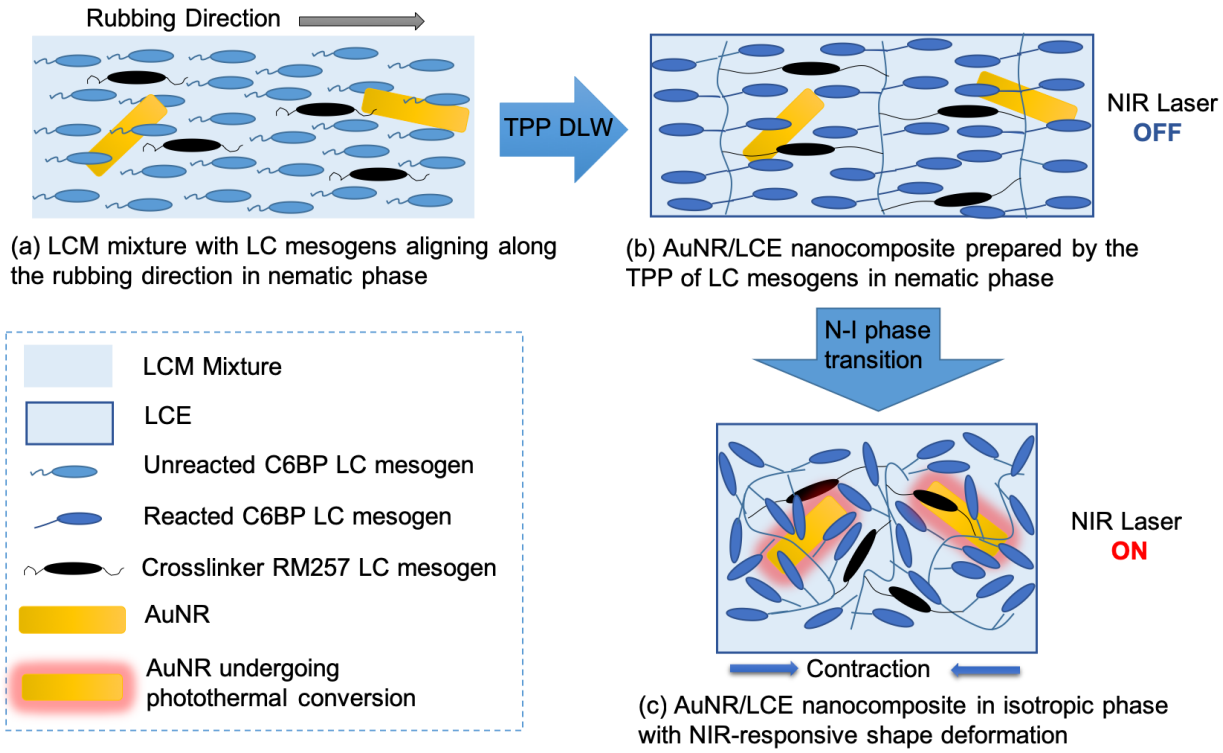

3.6.1 Effect of AuNR Loading Fraction. To study the effect of the AuNR loading fraction on the photothermal actuation properties, NIR-response photothermal actuation experiments were performed on the unmodified LCE and AuNR/LCE with 1 wt.%, 2 wt.% and 3 wt.% AuNRs in the shape of woodpile structures. An NIR laser with an output power of 1 W was used as the light source. The actuation processes were recorded, and the frames from the video were extracted and analyzed using the *ImageJ* software. Figure 6 shows the percentage elongations in the x- and y- directions of the woodpiles, induced by the NIR laser. The x-direction is the rubbing direction of the liquid crystal cell, along which the LC mesogens were oriented. When

the laser was switched on, the mesogens underwent N-to-I transition. The structure contracted along the x- direction and elongated along the y- direction. Notably, the percentage elongation of the AuNR/LCE increased with an increase in the amount of AuNRs. The LCE with 3 wt.% AuNRs demonstrated the largest deformation, in both the x- (9.5 %) and y- (-8.3 %) directions. At the same time, the unmodified LCE specimen demonstrated only a very small deformation, with the percentage elongations in the x- and y-directions being 1.2 % and -0.1 %, respectively. These results indicate that the photothermal effect of AuNRs can facilitate the N-to-I transition and induce a change in shape. A higher AuNR fraction in LCE generated a larger amount of thermal energy at a faster rate, which made the LCE jump to T_{NI} and more LC mesogens undergo N-to-I transition, leading to a larger deformation. The laser printed AuNR/LCE microstructures demonstrated excellent reversible-response as they could restore to 98.3–99.9 % of their original shapes after the NIR light was switched off.

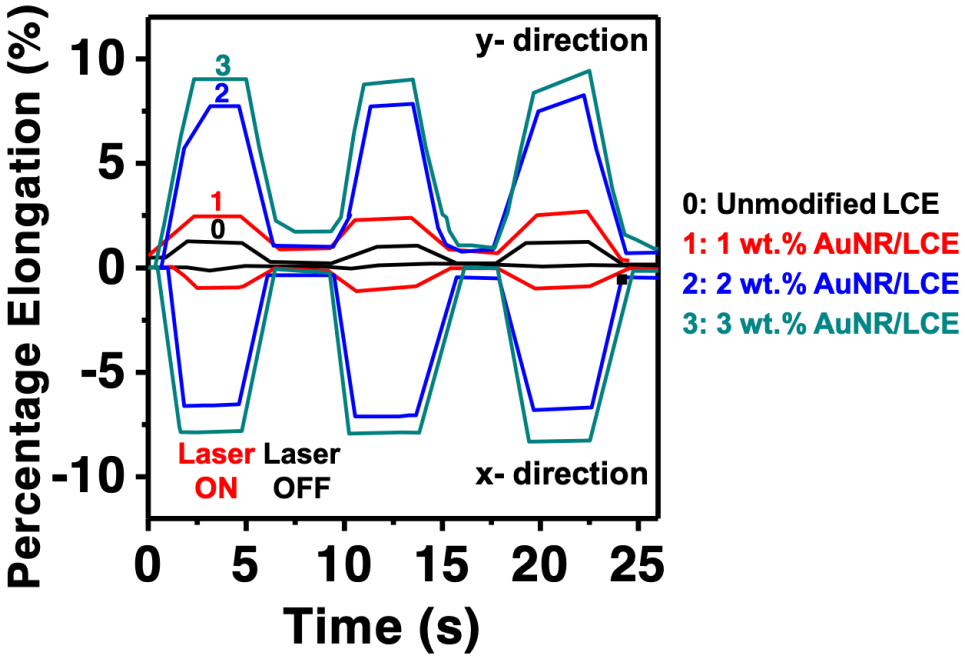

Figure 6. Percentage elongation of AuNR/LCE woodpile structures with different AuNR fractions (0–3 wt.%) induced by NIR irradiation with a laser power of 1 W.

3.6.2 Effect of Laser Power. To examine the effect of laser power, woodpile structures with 3 wt.% AuNR/LCE were used. The laser power was varied from 0.5 W to 2.5 W. Figure 7a shows that the percentage elongations in the x- and y- directions increased with increase in the laser power, especially in the range of 0.75 W to 1 W. The percentage elongations in the x- and y- directions were -18 % and 13 %, respectively, at 2 W. When the laser power was more than 2 W, no significant difference among those elongations was noted. Therefore, a laser power of 2 W was selected for further study of the actuation. Figure 7b shows the deformation and restoration saturated times of the 3 wt.% AuNR/LCE woodpile structures stimulated by different laser powers. When the AuNR/LCE sample was exposed to the NIR laser, the response time was less than one second, and the deformation-saturated time decreased from 4.5 s to 0.8 s when the laser power increased from 0.5 W to 2.5 W. In contrast, the shape restoration-saturated time increased from 1.5 s to 3.7 s. This finding suggests that a larger laser power induces faster deformation rates but slower restoration rates because a longer time is required for a greater amount of thermal energy to be dissipated. It is worth noting that when the laser power was 2 W, the deformation and restoration times were 0.9 s and 2.5 s, respectively. Further increase in the laser power had little effect on the deformation time (< 0.1 s), which suggests that the laser power of 2 W is an optimum value for evaluating the photothermal actuation performance, which could induce maximum strain within a relatively short time and thus facilitate rapid restoration of the structure to the original shape.

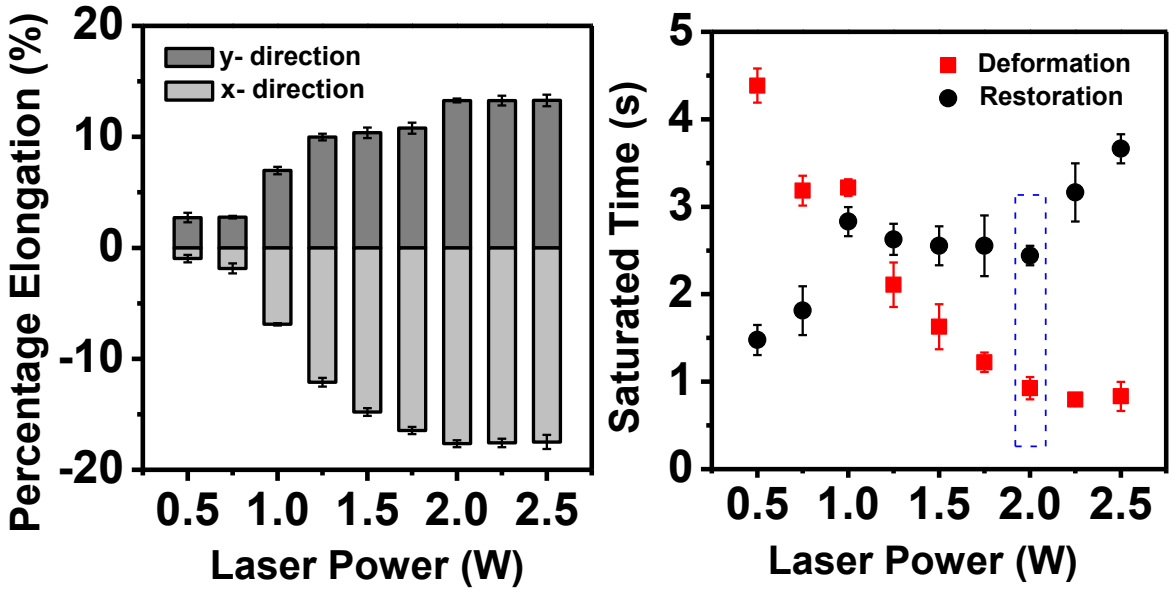

(a) (b)

Figure 7. (a) Percentage elongation in the x- and y- directions, (b) shape deformation and restoration saturated time of 3 wt.% AuNR/LCE woodpile structures when exposed and unexposed to NIR laser irradiation with power varied from 0.5 W to 2.5 W.

3.6.3 Stability of AuNR/LCE for Long-Term NIR Response. To investigate the stability of the AuNR/LCE nanocomposites, a multicycle actuation test was performed on the 3 wt.% AuNR/LCE reference structure. The changes in the actuation magnitude were recorded for 300 on-off switching cycles of NIR light with a period of five seconds. The corresponding result is shown in Figure 8. The photothermal actuation for the first 30 cycles is shown in Movie S1. Figure 8a shows the micrographs of the shape deformation and restoration of the AuNR/LCE woodpile structure during the 1st actuation cycle. Contraction in the x- direction (rubbing direction), leading to an elongation in the y- direction was observed when the NIR was switched on. The length in the x- direction of the woodpile structures, denoted as W in Figure 8a, was

monitored during the actuation process. Figures 8b and c show that the photothermal actuation started immediately when the NIR was switched on, and the maximum contraction was produced within 1 s. When the laser was switched off, the specimen restored to its original shape in approximately 4 s. Within the first few cycles, the magnitude of contraction (x- direction) was approximately 20 %, which is comparable to that of the LCE microscopic walkers with azobenzene units.[10] After 300 cycles, the magnitude of contraction reduced to 16 % and the photomechanical response rate was reduced, as shown in Figure 8b, according to the gradients of the curve at the time immediately after the NIR was switched on. The variation under multiple cycles may be attributed to the following reasons: (1) AuNRs are considerably stronger than LCE mechanically. The deterioration of the interface between the AuNRs and LCE matrix may occur due to the strain generated by the localized large deformation. As a result, the heat transfer becomes inefficient and the response rate is reduced; (2) movement and entanglement of molecules in multicycle actuation can cause a certain permanent deformation of the soft LCE matrix; and (3) multicycle actuation can increase the bulk temperature of the specimen. This effect reduces the temperature difference within a cycle of actuation, and the magnitude and rate of response are consequently reduced. The long-term evaluation of photoactuation properties of polymer-based materials is not easily found in the open literature. This work can provide useful reference for the durability of soft materials such as LCEs.

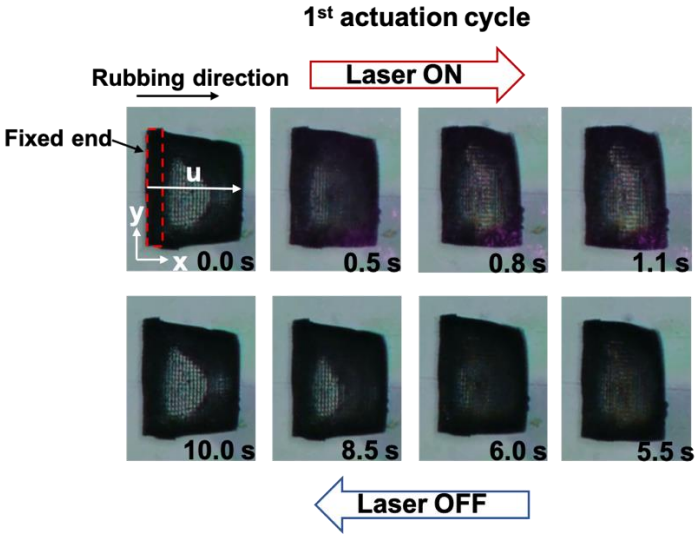

(a)

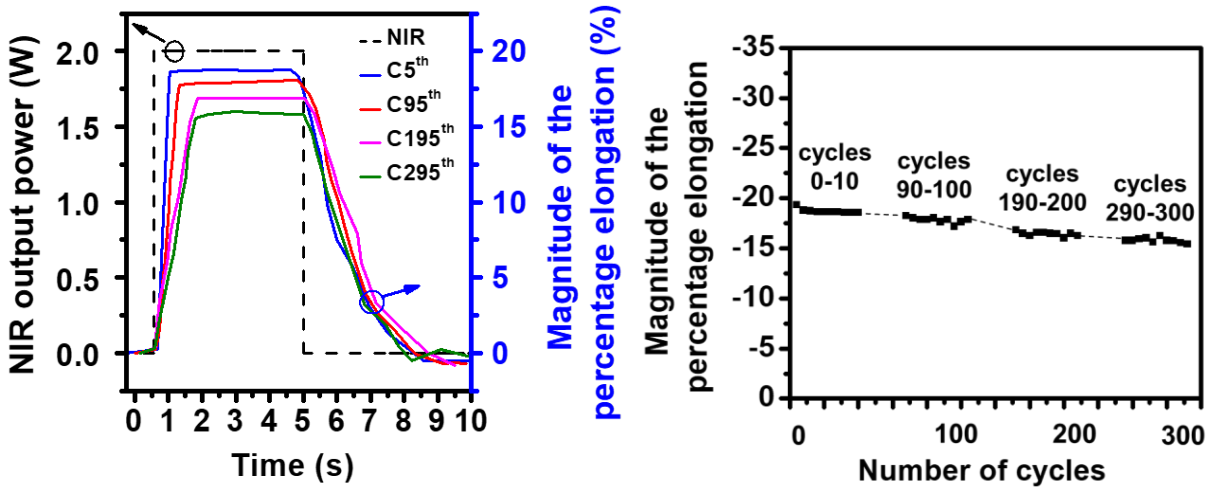

(b) (c)

Figure 8. (a) Micrographs of the shape deformation and restoration of the 3 wt.% AuNR/LCE woodpile structure during the 1st actuation cycle; (b) Magnitude of the percentage elongation of the 3 wt.% AuNR/LCE woodpile specimen in the x- direction at the 5th, 95th, 195th and 295th cycles, and (c) corresponding magnitude for 300 cycles.

3.7 Printability of Light-Powered AuNR-Modified LCE Nanocomposites

To study the printability of the AuNR-modified photoresist, different AuNR/LCE microstructures, such as hexagonal photonic crystal structure, frame structures and microclamps were printed, and they are shown in Figure 9. The resolution of the DLW of AuNR/LCE was found to be 1 μm based on the finest printable structural feature. Shrinkage could be observed after the development process. The shrinkage rate of the printed structure has been discussed in Section 2.8. Due to the effect of the shrinkages, shape distortion caused by the bending of truss members could be observed. To the best of our knowledge, most reported LCE-based actuators have pillar, fiber, cylinder or film forms. In this work, complex AuNR/LCE 3D microstructures were successfully fabricated using the proposed modified photoresist.

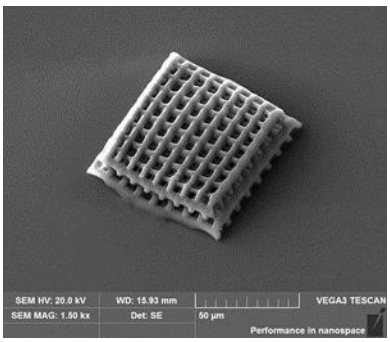

(a)

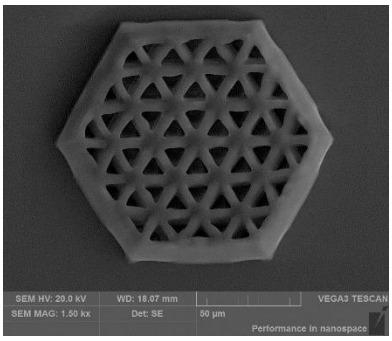

(b)

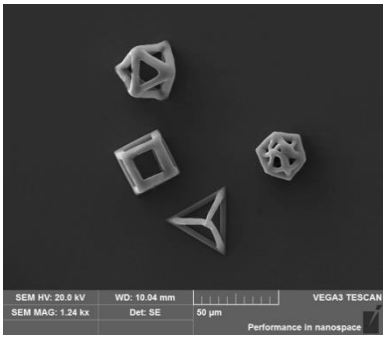

(c)

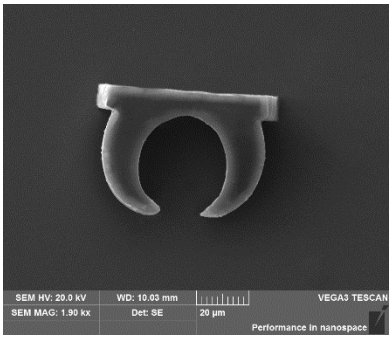

(d)

Figure 9. SEM images of the 3 wt.% AuNR/LCE 3D microstructures fabricated using DLW (a) woodpile structure, (b) hexagonal photonic crystal structure, (c) frame structures, (d) microclamp structures.

The microclamp shown in Figure 9d was designed and fabricated as a sample microdevice. The NIR-responsive photothermal actuation of this device was investigated and recorded. The actuation responses of the microclamp observed from both the top view and side view are shown in Movie S2 and Movie S3, respectively. The two arms of the clamp move toward the middle when exposed to the NIR. This clamp can potentially be used for clamping or gripping small items. The distance between the stage and the end point of the arms was measured for examining the dimensional changes. It was observed that the shape changed instantly with the laser actuation, and the maximum shape deformation occurred at approximately 40 %. The shape change implies that N-to-I phase transition of the LCE induced by the photothermal effect of AuNRs occurred. After the NIR laser was removed, the microclamp underwent shape restoration and returned to its original shape in only 0.5 s. These observations suggest that a 4D printable photoresist was developed successfully, and it could be printed into different types of structures via TPP with light-induced actuating properties.

4 CONCLUSION

A 4D printable "azobenzene-free" light-powered nanocomposite was prepared by the incorporation of AuNRs in LCEs, in which the AuNRs played two key roles: (i) as an efficient NIR absorber and photothermal agent that conferred light responsive capability; and (ii) as a nanofiller that enhanced the mechanical properties of the nanocomposites. Functionalizing the AuNR surfaces with MPA is a crucial step to make AuNRs miscible with LCEs and to realize different 3D microstructures by using TPP DLW. The appropriate printing parameters were

determined by a parameter sweep. In particular, photonic woodpile structures with 1–3 wt.% of AuNRs were prepared, and they demonstrated rapid reversible shape change. With the inclusion of 3 wt.% of AuNRs, the woodpile structure demonstrated a maximum percentage elongation of 20 % under the irradiation of a 2 W NIR laser and a rapid response time of less than 1 s. The nanocomposites demonstrated satisfactory stability after a long-term actuation cycle, as the magnitude of contraction was reduced by only 20 %. The material developed in this work could be easily adapted and extended to various applications. For example, because the microactuation can be controlled individually by a remote NIR source, microfilters and micropumps in a microfluidic system could be designed. In addition, nano-DMA was conducted to enable a deeper understanding of the mechanical properties of AuNR/LCE. The results indicated that a mechanical improvement of more than 80 % occurred due to the inclusion of AuNRs. The novel strategy reported in this study can be used for fabricating a variety of complex 3D microstructures, which can be used as high-performance micro-actuators or robotic devices in MEMS/NEMS and biomedical applications. The future directions of this work include: (1) the development of printable photoresists with more controllable mechanical properties (considering that LCEs are soft materials), and (2) the development and realization of functional 4D metamaterials and devices.

ASSOCIATED CONTENT

Supporting Information

Supporting Information is available from the ACS Publications website or from the author.

The following files are available free of charge:

Dispersion state of AuNRs in LCMs, DSC and TGA thermograms of AuNR/LCM mixtures, a woodpile structure designed for studying the actuation performance (PDF)

Photothermal actuation of the 3 wt.% AuNR/LCE woodpile structure via a chopped NIR laser for the first 35 cycles in air (MP4)

Photothermal actuation of the microclamp via a chopped NIR laser, both side view and top view (MP4)

AUTHOR INFORMATION

Corresponding Author

Chak Yin Tang

Tel.: +852 2766 6608

E-mail: cy.tang@polyu.edu.hk

Funding Sources

The work described in this paper was fully supported by a grant from the Research Grants Council of the Hong Kong Special Administrative Region, China (Project No. PolyU 15229716).

Notes

The authors have no conflicts of interest to declare.

ACKNOWLEDGMENTS

REFERENCES

(1) Marino, A.; Ciofani, G.; Filippeschi, C.; Pellegrino, M.; Pellegrini, M.; Orsini, P.; Pasqualetti, M.; Mattoli, V.; Mazzolai, B. Two-Photon Polymerization of Sub-micrometric Patterned Surfaces: Investigation of Cell-Substrate Interactions and Improved Differentiation of Neuron-like Cells. *ACS Appl. Mater. Interfaces* **2013,** *5*, 13012–13021.

(2) Meza, L. R.; Das, S.; Greer, J. R. Strong, Lightweight, and Recoverable Three-Dimensional Ceramic Nanolattices. *Science* **2014,** *345*, 1322–1326.

(3) Worthington, K. S.; Wiley, L. A.; Kaalberg, E. E.; Collins, M. M.; Mullins, R. F.; Stone, E. M.; Tucker, B. A. Two-Photon Polymerization for Production of Human iPSC-Derived Retinal Cell Grafts. *Acta Biomater.* **2017,** *55*, 385–395.

(4) Spangenberg, A.; Hobeika, N.; Stehlin, F.; Malval, J. P.; Wieder, F.; Prabhakaran, P.; Baldeck, P.; Soppera, O., Recent Advances in Two-Photon Stereolithography. In *Updates in Advanced Lithography*, Hosaka, S., Ed.; IntechOpen: London, UK, 2013; pp 35–63.

(5) Maruo, S.; Nakamura, O.; Kawata, S. Three-Dimensional Microfabrication with Two-Photon-Absorbed Photopolymerization. *Opt. Lett.* **1997,** *22*, 132–134.

(6) Liu, Y.; Nolte, D. D.; Pyrak-Nolte, L. J. Large-Format Fabrication by Two-Photon Polymerization in SU-8. *Appl. Phys. A* **2010,** *100*, 181–191.

(7) Torgersen, J.; Qin, X.-H.; Li, Z.; Ovsianikov, A.; Liska, R.; Stampfl, J. Hydrogels for Two-Photon Polymerization: A Toolbox for Mimicking the Extracellular Matrix. *Adv. Funct. Mater.* **2013,** *23*, 4542–4554.

(8) Dinca, V.; Kasotakis, E.; Catherine, J.; Mourka, A.; Ranella, A.; Ovsianikov, A.; Chichkov, B. N.; Farsari, M.; Mitraki, A.; Fotakis, C. Directed Three-Dimensional Patterning of Self-Assembled Peptide Fibrils. *Nano Lett.* **2008,** *8*, 538–543.

(9) Barner-Kowollik, C.; Bastmeyer, M.; Blasco, E.; Delaittre, G.; Müller, P.; Richter, B.; Wegener, M. 3D Laser Micro-and Nanoprinting: Challenges for Chemistry. *Angew. Chem., Int. Ed.* **2017,** *56*, 15828–15845.

(10) Zieger, M. M.; Müller, P.; Blasco, E.; Petit, C.; Hahn, V.; Michalek, L.; Mutlu, H.; Wegener, M.; Barner-Kowollik, C. A Subtractive Photoresist Platform for Micro- and Macroscopic 3D Printed Structures. *Adv. Funct. Mater.* **2018,** *28*, 1801405.

(11) Zeng, H.; Wasylczyk, P.; Parmeggiani, C.; Martella, D.; Burresi, M.; Wiersma, D. S. Light-Fueled Microscopic Walkers. *Adv. Mater.* **2015,** *27*, 3883–3887.

(12) Nocentini, S.; Martella, D.; Parmeggiani, C.; Wiersma, D. Photoresist Design for Elastomeric Light Tunable Photonic Devices. *Materials* **2016,** *9*, E525.

(13) Qing, X.; Qin, L.; Gu, W.; Yu, Y. Deformation of Cross-Linked Liquid Crystal Polymers by Light–From Ultraviolet to Visible and Infrared. *Liq. Cryst.* **2016,** *43*, 2114–2135.

(14) Brömmel, F.; Kramer, D.; Finkelmann, H., Preparation of Liquid Crystalline Elastomers. In *Liquid Crystal Elastomers: Materials and Applications*, de Jeu, W. H., Ed.; Springer: Berlin, Heidelberg, 2012; pp 1–48.

(15) Tian, H.; Wang, Z.; Chen, Y.; Shao, J.; Gao, T.; Cai, S. Polydopamine-Coated Main-Chain Liquid Crystal Elastomer as Optically Driven Artificial Muscle. *ACS Appl. Mater. Interfaces* **2018,** *10*, 8307–8316.

(16) Ohm, C.; Brehmer, M.; Zentel, R. Liquid Crystalline Elastomers as Actuators and Sensors. *Adv. Mater.* **2010,** *22*, 3366–3387.

(17) Guin, T.; Settle, M. J.; Kowalski, B. A.; Auguste, A. D.; Beblo, R. V.; Reich, G. W.; White, T. J. Layered Liquid Crystal Elastomer Actuators. *Nat. Commun.* **2018,** *9*, 2531.

(18) Jiang, H.; Li, C.; Huang, X. Actuators Based on Liquid Crystalline Elastomer Materials. *Nanoscale* **2013,** *5*, 5225–5240.

(19) Ahn, C.; Li, K.; Cai, S. Light or Thermally Powered Autonomous Rolling of an Elastomer Rod. *ACS Appl. Mater. Interfaces* **2018,** *10*, 25689–25696.

(20) Yu, Y.; Nakano, M.; Shishido, A.; Shiono, T.; Ikeda, T. Effect of Cross-linking Density on Photoinduced Bending Behavior of Oriented Liquid-Crystalline Network Films Containing Azobenzene. *Chem. Mater.* **2004,** *16*, 1637–1643.

(21) van Oosten, C. L.; Bastiaansen, C. W. M.; Broer, D. J. Printed Artificial Cilia from Liquid-Crystal Network Actuators Modularly Driven by Light. *Nat. Mater.* **2009,** *8*, 677–682.

(22) Palagi, S.; Mark, A. G.; Reigh, S. Y.; Melde, K.; Qiu, T.; Zeng, H.; Parmeggiani, C.; Martella, D.; Sanchez-Castillo, A.; Kapernaum, N.; Giesselmann, F.; Wiersma, D. S.; Lauga, E.; Fischer, P. Structured Light Enables Biomimetic Swimming and Versatile Locomotion of Photoresponsive Soft Microrobots. *Nat. Mater.* **2016,** *15*, 647–653.

(23) Zeng, H.; Martella, D.; Wasylczyk, P.; Cerretti, G.; Lavocat, J.-C. G.; Ho, C.-H.; Parmeggiani, C.; Wiersma, D. S. High-Resolution 3D Direct Laser Writing for Liquid-Crystalline Elastomer Microstructures. *Adv. Mater.* **2014,** *26*, 2319–2322.

(24) Fomina, N.; McFearin, C. L.; Sermsakdi, M.; Morachis, J. M.; Almutairi, A. Low Power, Biologically Benign NIR Light Triggers Polymer Disassembly. *Macromolecules* **2011,** *44*, 8590–8597.

(25) Wu, W.; Yao, L.; Yang, T.; Yin, R.; Li, F.; Yu, Y. NIR-Light-Induced Deformation of Cross-Linked Liquid-Crystal Polymers Using Upconversion Nanophosphors. *J. Am. Chem. Soc.* **2011,** *133*, 15810–15813.

(26) Wang, X.; Liu, X.; Wang, L.; Tang, C.-Y.; Law, W.-C.; Zhang, G.; Liao, Y.; Liu, C.; Liu, Z. Synthesis of Yolk–Shell Polymeric Nanocapsules Encapsulated with Monodispersed Upconversion Nanoparticle for Dual-Responsive Controlled Drug Release. *Macromolecules* **2018,** *51*, 10074–10082.

(27) Camargo, C. J.; Campanella, H.; Marshall, J. E.; Torras, N.; Zinoviev, K.; Terentjev, E. M.; Esteve, J. Localised Actuation in Composites Containing Carbon Nanotubes and Liquid Crystalline Elastomers. *Macromol. Rapid Commun.* **2011,** *32*, 1953–1959.

(28) Cheng, Z.; Wang, T.; Li, X.; Zhang, Y.; Yu, H. NIR–Vis–UV Light-Responsive Actuator Films of Polymer-Dispersed Liquid Crystal/Graphene Oxide Nanocomposites. *ACS Appl. Mater. Interfaces* **2015,** *7*, 27494–27501.

(29) Yang, Y.; Zhan, W.; Peng, R.; He, C.; Pang, X.; Shi, D.; Jiang, T.; Lin, Z. Graphene-Enabled Superior and Tunable Photomechanical Actuation in Liquid Crystalline Elastomer Nanocomposites. *Adv. Mater.* **2015,** *27*, 6376–6381.

(30) Yang, L.; Setyowati, K.; Li, A.; Gong, S.; Chen, J. Reversible Infrared Actuation of Carbon Nanotube-Liquid Crystalline Elastomer Nanocomposites. *Adv. Mater.* **2008,** *20*, 2271–2275.

(31) Becerril, H. A.; Mao, J.; Liu, Z.; Stoltenberg, R. M.; Bao, Z.; Chen, Y. Evaluation of Solution-Processed Reduced Graphene Oxide Films as Transparent Conductors. *ACS Nano* **2008,** *2*, 463–470.

(32) Li, C.; Liu, Y.; Huang, X.; Li, C.; Jiang, H. Light Actuation of Graphene-Oxide Incorporated Liquid Crystalline Elastomer Nanocomposites. *Mol. Cryst. Liq. Cryst.* **2015,** *616*, 83–92.

(33) Zhang, S.-J.; Li, Y.; Wang, Y.-K.; Liu, L.-P.; Wang, H.-D.; Xiao, Y.-F.; Yang, H.; Gong, Q. Controlling Young's Modulus of Polymerized Structures Fabricated by Direct Laser Writing. *Appl. Phys. A* **2015,** *118*, 437–441.

(34) Lemma, E. D.; Rizzi, F.; Dattoma, T.; Spagnolo, B.; Sileo, L.; Qualtieri, A.; De Vittorio, M.; Pisanello, F. Mechanical Properties Tunability of Three-Dimensional Polymeric Structures in Two-Photon Lithography. *IEEE Trans. Nanotechnol.* **2017,** *16*, 23–31.

(35) Shin, C.-S.; Li, T.-J.; Lin, C.-L. Alleviating Distortion and Improving the Young's Modulus in Two-Photon Polymerization Fabrications. *Micromachines* **2018,** *9*, E615.

(36) Liu, X.; Wei, R.; Hoang, P. T.; Wang, X.; Liu, T.; Keller, P. Reversible and Rapid Laser Actuation of Liquid Crystalline Elastomer Micropillars with Inclusion of Gold Nanoparticles. *Adv. Funct. Mater.* **2015,** *25*, 3022–3032.

(37) Montazami, R.; Spillmann, C. M.; Naciri, J.; Ratna, B. R. Enhanced Thermomechanical Properties of a Nematic Liquid Crystal Elastomer Doped with Gold Nanoparticles. *Sens. Actuators, A* **2012,** *178*, 175–178.

(38) Sun, Y.; Evans, J. S.; Lee, T.; Senyuk, B.; Keller, P.; He, S.; Smalyukh, I. I. Optical Manipulation of Shape-Morphing Elastomeric Liquid Crystal Microparticles Doped with Gold Nanocrystals. *Appl. Phys. Lett.* **2012,** *100*, 241901.

(39) Yang, H.; Liu, J.-J.; Wang, Z.-F.; Guo, L.-X.; Keller, P.; Lin, B.-P.; Sun, Y.; Zhang, X.-Q. Near-Infrared-Responsive Gold Nanorod/Liquid Crystalline Elastomer Composites Prepared by Sequential Thiol-Click Chemistry. *Chem. Commun.* **2015,** *51*, 12126–12129.

(40) Vigderman, L.; Zubarev, E. R. High-Yield Synthesis of Gold Nanorods with Longitudinal SPR Peak Greater than 1200 nm Using Hydroquinone as a Reducing Agent. *Chem. Mater.* **2013,** *25*, 1450–1457.

(41) Xiao, Z.; Wu, Q.; Luo, S.; Zhang, C.; Baur, J.; Justice, R.; Liu, T. Shape Matters: A Gold Nanoparticle Enabled Shape Memory Polymer Triggered by Laser Irradiation. *Part. Part. Syst. Charact.* **2013,** *30*, 338–345.

(42) Nguyen, A. K.; Narayan, R. J. Two-Photon Polymerization for Biological Applications. *Mater. Today* **2017,** *20*, 314–322.

(43) Xing, J.-F.; Dong, X.-Z.; Chen, W.-Q.; Duan, X.-M.; Takeyasu, N.; Tanaka, T.; Kawata, S. Improving Spatial Resolution of Two-Photon Microfabrication by Using Photoinitiator with High Initiating Efficiency. *Appl. Phys. Lett.* **2007,** *90*, 131106.

(44) Chen, L.; Wang, J. X.; Tang, C. Y.; Chen, D. Z.; Law, W. C. Shape Memory Effect of Thermal-Responsive Nano-Hydroxyapatite Reinforced Poly-D-L-lactide Composites with Porous Structure. *Composites, Part B* **2016,** *107*, 67–74.

(45) Chen, L.; Tang, C. Y.; Chen, D. Z.; Wong, C. T.; Tsui, C. P. Fabrication and Characterization of Poly-D-L-Lactide/Nano-Hydroxyapatite Composite Scaffolds with Poly (Ethylene Glycol) Coating and Dexamethasone Releasing. *Compos. Sci. Technol.* **2011,** *71*, 1842–1849.

(46) Sen, S.; Thomin, J. D.; Kumar, S. K.; Keblinski, P. Molecular Underpinnings of the Mechanical Reinforcement in Polymer Nanocomposites. *Macromolecules* **2007,** *40*, 4059–4067.

(47) Chen, L.; Tang, C. Y.; Tsui, C. P.; Chen, D. Z. Mechanical Properties and In Vitro Evaluation of Bioactivity and Degradation of Dexamethasone-Releasing Poly-D-L-Lactide/Nano-Hydroxyapatite Composite Scaffolds. *J. Mech. Behav. Biomed. Mater.* **2013,** *22*, 41–50.

(48) Richter, S.; Kreyenschulte, H.; Saphiannikova, M.; Götze, T.; Heinrich, G. Studies of the So-Called Jamming Phenomenon in Filled Rubbers Using Dynamical-Mechanical Experiments. *Macromol. Symp.* **2011,** *306-307*, 141–149.

(49) Zaragoza, J.; Fukuoka, S.; Kraus, M.; Thomin, J.; Asuri, P. Exploring the Role of Nanoparticles in Enhancing Mechanical Properties of Hydrogel Nanocomposites. *Nanomaterials* **2018,** *8*, E882.

Table of Contents Graphic

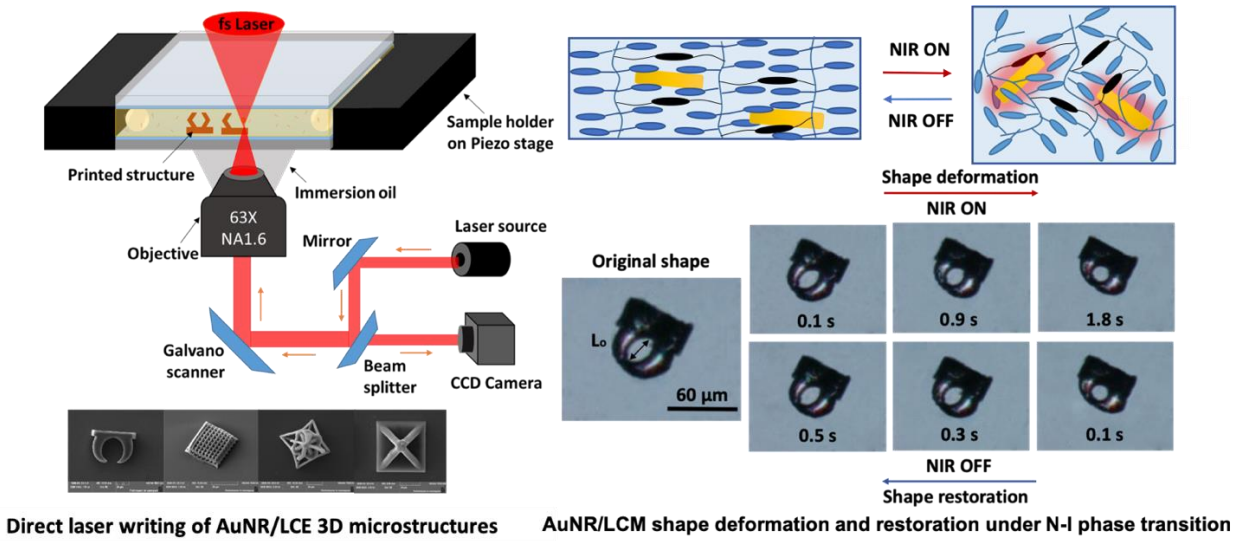

Direct laser writing of AuNR/LCE 3D microstructures

AuNR/LCM shape deformation and restoration under N-I phase transition